

Astronomy & Astrophysics manuscript no.  
(will be inserted by hand later)

# Antiprotons from primordial black holes

Aurélien Barrau<sup>1,3</sup>, Gaëlle Boudoul<sup>1,3</sup>, Fiorenza Donato<sup>2</sup>, David Maurin<sup>2</sup>,  
Pierre Salati<sup>2,4</sup>, Richard Taillet<sup>2,4</sup>

<sup>1</sup> ISN Grenoble, 53 av des Martyrs, 38026 Grenoble cedex, France

<sup>2</sup> LAPTH, B.P. 110 Annecy-le-Vieux, 74941, France

<sup>3</sup> Université Joseph Fourier, Grenoble, 38000, France.

<sup>4</sup> Université de Savoie, Chambéry, 73011, France.

Received;Accepted

**Abstract.** Primordial black holes (PBHs) have motivated many studies since it was shown that they should evaporate and produce all kinds of particles (Hawking 1974). Recent experimental measurements of cosmic rays with great accuracy, theoretical investigations on the possible formation mechanisms and detailed evaporation processes have revived the interest in such astrophysical objects. This article aims at using the latest developments on antiproton propagation models (Maurin et al. 2001 and Donato et al. 2001a) together with new data from BESS, CAPRICE and AMS experiments to constrain the local amount of PBH dark matter. Depending on the diffusion halo parameters and on the details of emission mechanism, we derive an average upper limit of the order of  $\rho_{\odot}^{PBH} \approx 1.7 \cdot 10^{-33} \text{ g cm}^{-3}$ .

**Key words.** Cosmic rays - Black hole physics - Dark matter

## 1. Introduction

Very small black holes could have formed in the early universe from initial density inhomogeneities (Hawking 1971), from phase transition (Hawking 1982), from collapse of cosmic strings (Hawking 1989) or as a result of a softening of the equation of state (Canuto 1978). It was also shown by Choptuik (1993) and, more recently, studied in the framework of double inflation (Kim 2000), that PBHs could have formed by near-critical collapse in the expanding universe. This later case is of particular interest as it generates a scaling mass relation similar to that of black holes produced in asymptotically flat spacetime, *i.e.* with a wide range of masses at a given formation time. Depending on

*Send offprint requests to:* A. Barrau

*Correspondence to:* Aurelien.Barrau@cern.ch

the details of the model chosen and on the reheating temperature (in the inflationary framework), the mass distribution of PBHs can therefore be significantly different from the usual  $M^{-5/2}$  power law (Carr 1975) between Planck value and infinity.

The interest in primordial black holes was clearly revived in the last years for several reasons. First, new experimental data on gamma-rays (Connaughton 1998) and cosmic rays (Maki *et al.* 1996) together with the construction of neutrinos detectors (Bugaev & Konishchev 2001), of extremely high-energy particle observatories (Barrau 2000) and of gravitational waves interferometers (Nakamura *et al.* 1997) give interesting investigation means to look for indirect signatures of PBHs. Then, primordial black holes have been used to derive a quite stringent limit on the spectral index of the initial scalar perturbation power spectrum due to a dust-like phase of the cosmological expansion (Kotok & Naselsky 1998). It was also found that PBHs are a great probe of the early universe with a varying gravitational constant (Carr 2001). Finally, significant progress have been made in the understanding of the evaporation mechanism itself, both at usual energies (Parikh & Wilczek 2000) and in the near-planckian tail of the spectrum (Barrau & Alexeyev 2001, Alexeyev *et al.* 2001).

Among other cosmic rays, antiprotons are especially interesting as their secondary flux (due to interactions of proton and helium nuclei with the interstellar medium) is both rather small (the  $\bar{p}/p$  ratio is lower than  $10^{-4}$  at all energies) and quite well known. This study aims at deriving new estimations of the PBH local density, taking into account the latest measurements of the antiproton spectrum and realistic models for cosmic ray propagation. Contrarily to what has been thought in early studies on antiproton spectra (see, *e.g.*, Gaisser & Schaefer 1992 for a review) and to what is still assumed in some recent PBH studies (*e.g.* Kanazawa *et al.* 2000) there is no need for any exotic astrophysical source to account for the measured  $\bar{p}$  flux. On the other hand, the very good agreement between experimental data and theoretical predictions with a purely secondary origin of antiprotons (see Donato *et al.* 2001a) allows to derive quite stringent upper limit on the amount of PBH dark matter. This article focuses on this point and is organised in the following way : the first section reminds general consideration on the evaporation process and on the subsequent fragmentation phenomena. The second part is devoted to the primary antiproton sources while the third part describes all propagation aspects, with a particular emphasis on the uncertainties coming from astrophysical parameters (mostly the magnetic halo thickness) and nuclear physics cross-sections. Next, the resulting “top of atmosphere” (TOA) antiproton spectra for different formation conditions and for different possible emission models are studied. Finally, we derive the resulting upper limits on the local PBH density and consider possible future developments both on the experimental and theoretical sides.

## 2. Antiproton emission from PBHs

### 2.1. Hawking process

The Hawking black hole evaporation process can be intuitively understood as a quantum creation of particles from the vacuum by an external field. The basic characteristics can be easily seen through a simplified model (see Frolov & Novikov 1998 for more details). Let  $\Gamma$  be the field strength and  $g$  the charge of the created particle. In the creation of a virtual pair, the probability  $P$  to find a particle at a distance greater than  $l$  from the other is proportional to  $\exp(-l/\lambda)$  with  $\lambda = \hbar/mc$  the Compton wavelength. The associated amplitude is non-vanishing only if  $l$  is such that the work of the field  $g\Gamma l$  is equal to  $2mc^2$ . It results in  $P \propto \exp(-2m^2c^3/\hbar g\Gamma)$ , which should be corrected by a factor  $\pi/2$  due to the fact that the quantity standing in the exponent is nothing else than the Euclidean action involved in a tunnelling process. Of course, the pre-factor and the accurate form of the argument depend on subtler characteristics of the field, but this framework allowed Schwinger to derive in 1951 the rate of particle production by a uniform electric field and remains correct, at the intuitive level, for black holes evaporation. If we focus on a static gravitational field, we must take into account that the energy of a particle can be written  $E = -p_\mu \xi^\mu$ , where  $p^\mu$  is the four-momentum and  $\xi^\mu$  is the Killing vector. The momentum being a future-directed timelike vector, the energy  $E$  is always positive in the regions where the Killing vector is also future-directed and timelike. If both particles were created in such a region, their total energy would not vanish and the process would, therefore, be forbidden by conservation of energy. As a result, a static gravitational field can create particles only in a region where the Killing vector is spacelike. Such a region lies inside the Killing horizon, *i.e.* the  $\xi^2 = 0$  surface, which is the event horizon in a static spacetime. This basic argument shows that particle creation by a gravitational field in a static spacetime (this is also true in a stationary case) is possible only if it contains a black hole. Although very similar to the effect of particle creation by an electric field, the Hawking process has a fundamental difference: since the states of negative energy are confined inside the hole, only one of the created particles can appear outside and reach infinity. This means that the classical observer has access to only a part of the total quantum system. The state of particles outside the black hole is, therefore, always described by a density matrix, even if, initially, the state of the quantum system was pure. It has important consequences regarding the ultimate fate of evaporating black holes.

To derive the accurate emission process, which mimics a Planck law, Hawking used the usual quantum mechanical wave equation for a collapsing object with a postcollapse classical curved metric instead of a precollapse Minkowski one (Hawking 1975). He found

that the emission spectrum for particles of energy  $Q$  per unit of time  $t$  is, for each degree of freedom:

$$\frac{d^2N}{dQdt} = \frac{\Gamma_s}{h \left( \exp \left( \frac{Q}{h\kappa/4\pi^2c} \right) - (-1)^{2s} \right)}$$

where contributions of electric potential and angular velocity have been neglected since the black hole discharges and finishes its rotation much faster than it evaporates (Gibbons 1975 and Page 1977).  $\kappa$  is the surface gravity,  $s$  is the spin of the emitted species and  $\Gamma_s$  is the absorption probability. If we introduce the Hawking temperature for a black hole of mass  $M$  (one of the rare physics formula using all the fundamental constants) defined by

$$T = \frac{hc^3}{16\pi kGM} \approx \frac{10^{13}g}{M} \text{GeV}$$

the argument of the exponent becomes simply a function of  $Q/kT$ . Although the absorption probability is often approximated by its relativistic limit

$$\lim_{Q \rightarrow \infty} \Gamma_s = \frac{108\pi^2 G^2 M^2 Q^2}{h^2 c^6}$$

we took into account in this work its real expression for non-relativistic particles:

$$\Gamma_s = \frac{4\pi\sigma_s(Q, M, \mu)}{h^2 c^2} (Q^2 - \mu^2)$$

where  $\sigma_s$  is the absorption cross-section computed numerically (Page 1976) and  $\mu$  the rest mass of the emitted particle. Even if the effect is partially compensated by the pseudo-oscillating behaviour of the cross-section (cf Fig. 1) and remains at the level of a correction, we found some substantial discrepancies between the geometric limit and the numerical calculation which justifies this technical complication.

## 2.2. Hadronization

As it was shown by MacGibbon and Webber (1990), when the black hole temperature is greater than the quantum chromodynamics confinement scale  $\Lambda_{QCD}$ , quarks and gluons jets are emitted instead of composite hadrons. To evaluate the number of emitted antiprotons, one therefore needs to perform the following convolution:

$$\frac{d^2N_{\bar{p}}}{dEdt} = \sum_j \int_{Q=E}^{\infty} \alpha_j \frac{\Gamma_j(Q, T)}{h} \left( e^{\frac{Q}{hT}} - (-1)^{2s_j} \right)^{-1} \times \frac{dg_{j\bar{p}}(Q, E)}{dE} dQ$$

where  $\alpha_j$  is the number of degrees of freedom,  $E$  is the antiproton energy and  $dg_{j\bar{p}}(Q, E)/dE$  is the normalized differential fragmentation function, *i.e.* the number of antiprotons between  $E$  and  $E + dE$  created by a parton jet of type  $j$  and energy  $Q$ . Of course, decays of heavy unstable particles (in our case antineutrons) must also be taken into account. The fragmentation functions have been evaluated with the high-energy physics frequently used event generator PYTHIA/JETSET (Tjöstrand 1994). This program is based on the so-called string fragmentation model (developed by the Lund group)

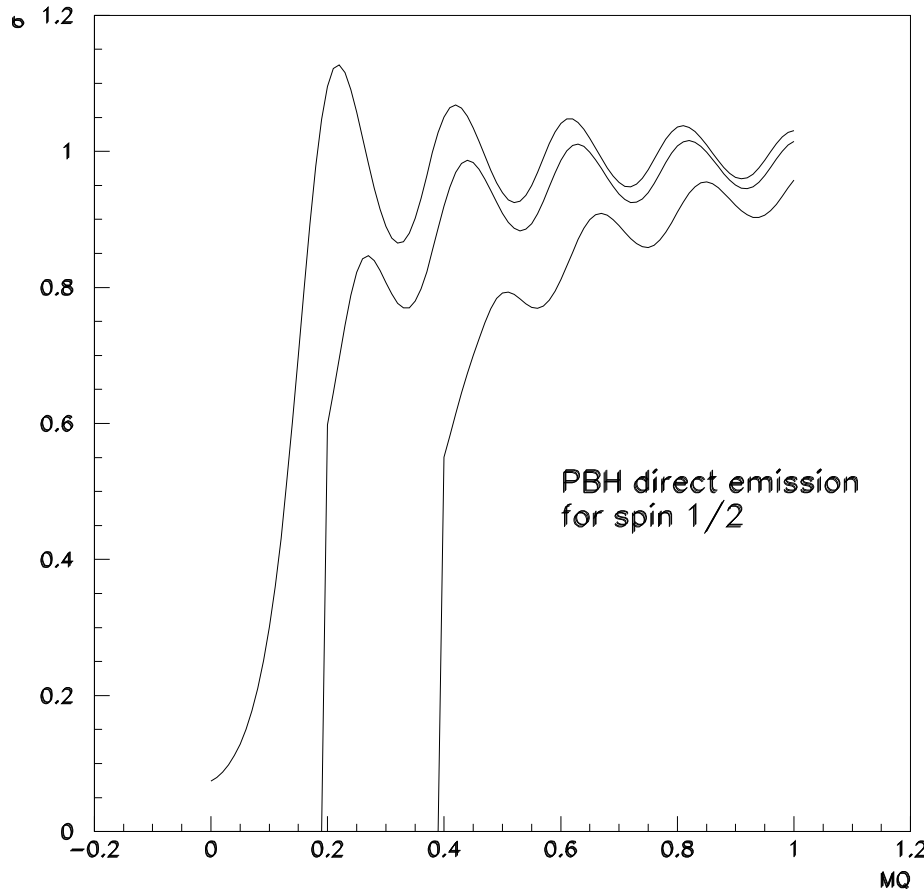


**Fig. 1.** Cross-sections in units of the high-energy limit (Page 1976) for the emission of a spin 1/2 particle of mass  $\mu$  and energy  $Q$  by a nonrotating uncharged black hole of mass  $M$ . Upper curve is for  $M\mu = 0$ , middle one for  $M\mu = 0.2$  and lower one for  $M\mu = 0.4$ . All numbers are in Planck units.

which is an explicit and detailed framework where the long-range confinement forces are allowed to distribute the energies and flavours of a parton configuration among a collection of primary hadrons. It has received many improvements related, *e.g.*, with parton showers, hard processes, Higgs mechanisms and it is now in excellent agreement with experimental data. Fig. 2 shows one of the fragmentation functions we have computed with PYTHIA.

### 3. Primary sources

In order to compute the antiproton spectrum for a given local PBH density, the number  $q_{\bar{p}}^{PBH}(r, z, E)$  of antiprotons emitted with kinetic energy between  $E$  and  $E + dE$  per unit volume and time, must be evaluated. It is proportional to the number  $d^2n/dMdV$ , of

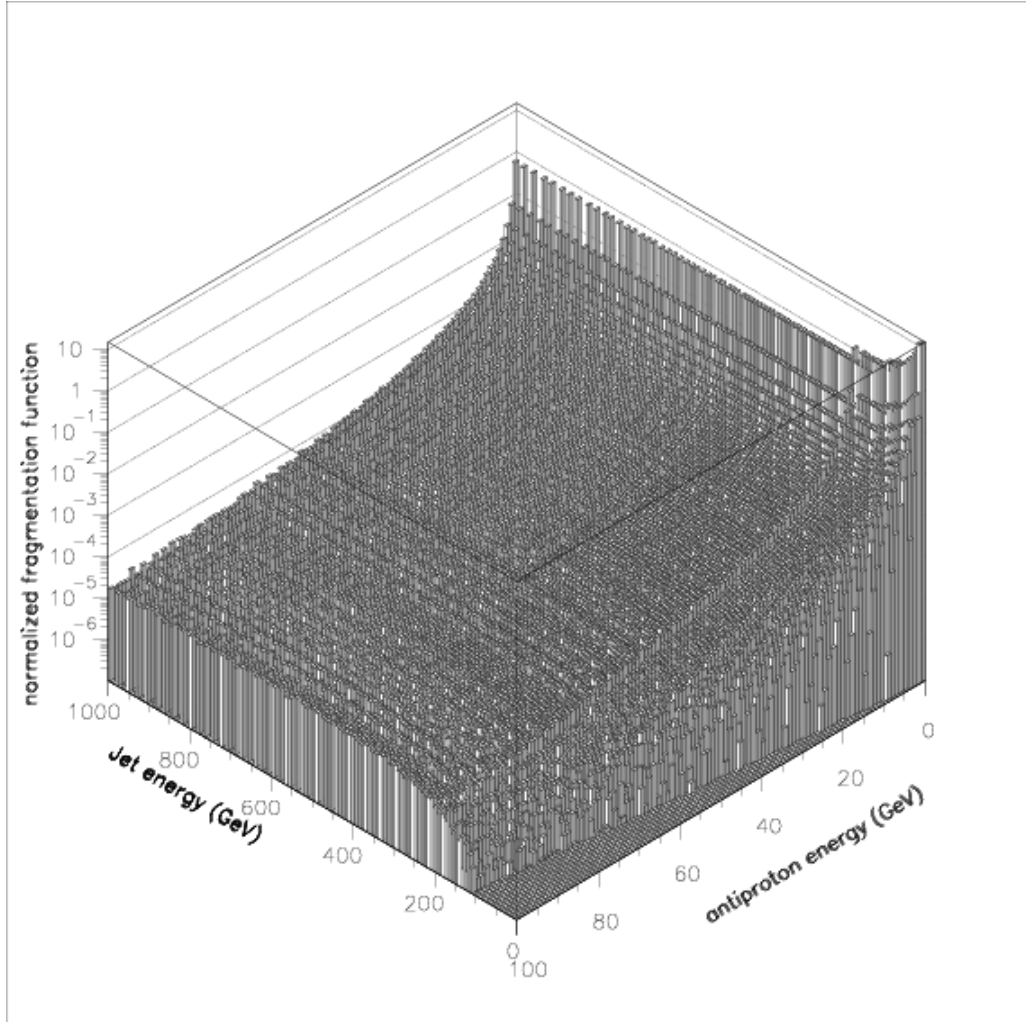


**Fig. 2.** Normalized fragmentation function for a gluon jet. X axis is the jet energy (GeV) and Y axis is the hadron energy (GeV).

PBHs per unit of mass and volume and to the individual flux  $d^2N_{\bar{p}}/dE dt$  emitted by one PBH, so that

$$q^{prim}(r, z, E) = \int \frac{d^2N_{\bar{p}}(M, E)}{dE dt} \cdot \frac{d^2n(r, z)}{dM dV} dM$$

where  $r$  and  $z$  are the cylindrical coordinates describing position in our Galaxy. As the physics of evaporation and the mass spectrum of PBH do not depend on their numerical density, the spatial dependence can be factored out as

$$\frac{d^2n(r, z)}{dM dV} = \frac{d^2n_{\odot}}{dM dV} \times f(r, z).$$

The function  $f(r, z)$  is determined by using

$$\rho(r, z)^{PBH} = \int_{M_{min}}^{M_{max}} \frac{d^2n(r, z)}{dM dV} M dM = f(r, z) \int_{M_{min}}^{M_{max}} \frac{d^2n_{\odot}}{dM dV} M dM = f(r, z) \rho_{\odot}^{PBH}$$

The primary source term can be split into a spatial and a spectral dependance, as

$$q^{prim}(r, z, E) = q^{prim}(r, z) \times Q^{PBH}(E) \quad (1)$$

with

$$q^{prim}(r, z) = \frac{\rho_{\odot}^{PBH}(r, z)}{\rho_{\odot}^{PBH}} \quad \text{and} \quad Q^{PHB}(E) = \int_{M_{min}}^{M_{max}} \frac{d^2 N_{\bar{p}}}{dE dt} \cdot \frac{d^2 n_{\odot}}{dM dV} dM \quad (2)$$

### 3.1. Spatial distribution

Primordial black holes should have followed the dark matter particles during the formation of halos, so that they may have the same spatial distribution. Unfortunately, this distribution is not very well known, and several independent evidences are contradictory. The first constraint on this distribution is that the observed rotation curve of our Galaxy is almost flat beyond a few kpc from the center. For a spherical halo, it follows that the density decreases as  $1/r^2$  outside the central regions (the bulge). As regards the bulge itself, the situation is far from clear. Numerical simulations indicate that the central distribution of dark matter is cuspy, with a  $r^{-\gamma}$  dependence with  $\gamma \sim 0.5 - 1.5$  (Ghez. *et al.* 1998, Gondolo & Silk 1999), but there is an indirect argument against this numerical result: most barred spiral galaxies have a so-called fast rotating bar, which is very unlikely if too much dark matter is present because dynamical friction would slow them down quite efficiently (Debattista and Sellwood 1998, 2000).

In the absence of a clear answer to this problem, several profiles for the PBH distribution can be used, with the generic form

$$\frac{\rho^{PBH}(r, z)}{\rho_{\odot}^{PBH}} = \left( \frac{R_{\odot}}{\sqrt{r^2 + z^2}} \right)^{\gamma} \left( \frac{R_c^{\alpha} + R_{\odot}^{\alpha}}{R_c^{\alpha} + (\sqrt{r^2 + z^2})^{\alpha}} \right)^{\epsilon} \quad (3)$$

if spherical symmetry is assumed.

Different cases have been considered, with numerical values taken in Calcáneo-Roldán and Moore (2001). Numerical simulations point toward singular profiles with  $\gamma = 1.5$ ,  $\alpha = 1.5$ ,  $\epsilon = 1$  and  $R_c = 33.2$  kpc (Moore 1999) or  $\gamma = 1$ ,  $\alpha = 1$ ,  $\epsilon = 2$  and  $R_c = 27.7$  kpc (Navarro, Frank & White 1996, hereafter NFW). We also considered an isothermal profile with  $\gamma = 0$ ,  $\alpha = 2$  and  $\epsilon = 1$  and a modified isothermal profile with  $\gamma = 0$ ,  $\alpha = 2$  and  $\epsilon = 1.5$  and  $R_c = 24.3$  kpc.

### 3.2. Spectral dependence

It can be seen from eq. (2) that the keypoints to derive the  $Q^{PBH}(E)$  term are the shape of the mass spectrum today and the boundaries of the integral. The choice of  $M_{min}$  and  $M_{max}$  is discussed later.

#### 3.2.1. PBH mass spectrum

The mass spectrum today is the result of the evolution of the initial mass spectrum in time. The usual picture is based on the idea that a PBH can form if an overdense region

collapses with the following conditions on the contrast density  $\delta$  (Harrison 1970, Carr & Hawking 1974):

$$1/3 \leq \delta \leq 1$$

The left inequality ensures that the considered region overcomes the Jeans pressure and the right one ensures that it does not become a decoupled universe. The initial spectrum can be analytically computed in this framework with the Press-Schechter method. For Gaussian fluctuations, the probability that a region of size  $R$  and mass  $M$  has a density contrast between  $\delta$  and  $\delta + d\delta$  is

$$P(M, \delta) d\delta = \frac{1}{\sigma_R(M)\sqrt{2\pi}} \exp\left(-\frac{\delta^2}{2\sigma_R^2(M)}\right) d\delta$$

where  $\sigma_M$  is the standard deviation of the regions with a comoving size  $R$  and mass  $M$ . After having related the amplitudes at the formation time to the amplitudes at the horizon crossing time, integrating the previous probability on the authorized range and changing the variable, it can be shown that (Carr 1975), in a radiation dominated universe, the initial mass spectrum is simply given by:

$$\left(\frac{dn}{dM_{init}}\right) \propto M_{init}^{-\frac{5}{2}}$$

This spectrum will be regarded as the *standard model* (see, *e.g.* Bugaev & Konishev 2001 for a review). To deduce the mass spectrum today from this initial one, the mass loss rate must be evaluated. It can be written as the integral of the product of the Hawking spectrum with the energy of the emitted particle and was shown to be (Page 1976) numerically approximated by:

$$\frac{dM}{dt} = \int_0^\infty \frac{\Gamma_s(Q, M) Q dQ}{h\left(\exp\left(\frac{Q}{kT}\right) - (-1)^{2s}\right)} \approx \frac{-\alpha(M)}{M^2}$$

where  $\alpha \approx \{7.8d_{s=1/2} + 3.1d_{s=1}\} \times 10^{24} \text{ g}^3 \text{ s}^{-1}$  with  $d_{s=1/2}$  and  $d_{s=1}$  the fermionic and bosonic degrees of freedom available for a given PBH temperature (Halzen *et al.* 1991). This  $M^{-2}$  behaviour can be easily understood when keeping in mind that  $\Gamma_s \propto Q^2$  at the geometric optic limit. If we approximate the previous law with  $\alpha \approx \text{const}$ , which is correct as far as the number of degrees of freedom does not increase dramatically fast, the mass can be written as a function of time as:

$$M_{init} \approx (3\alpha t + M^3)^{1/3}.$$

It is then straightforward to see that with

$$\frac{dn}{dM} = \frac{dn}{dM_{init}} \cdot \frac{dM_{init}}{dM}$$

the resulting spectrum today is characterised by

$$\frac{dn}{dM} \propto M^2 \text{ for } M < M_*$$

$$\frac{dn}{dM} \propto M^{-5/2} \text{ for } M > M_*$$

where  $M_* \approx 5 \times 10^{14} \text{ g}$  is the initial mass of a PBH expiring nowadays. In this model, the mass of a PBH formed at time  $t$  is determined by the horizon mass at this epoch,

$$M = \frac{1}{8} \frac{M_{Pl}}{t_{Pl}} t.$$

In the usual cosmological picture, only PBHs formed after inflation should be taken into account as those produced before would be extremely diluted due to the huge increase of the cosmic scale factor. The end-time of inflation  $t_{RH}$  being related to the reheating temperature  $T_{RH}$  by

$$t_{RH} \approx 0.3g^{-1/2} \frac{M_{Pl}}{T_{RH}^2}$$

where  $g \approx 100$  is the number of degrees of freedom in the early universe, the minimal mass of PBH in the initial spectrum can be given as a function  $T_{RH}$ .

It should be emphasized that the shape of the spectrum below  $M_* \approx (3at)^{1/3}$  does not depend on any assumption about the initial mass spectrum. Whatever the initial spectrum, it should increase as  $M^2$  today: this is only due to the  $dM_{init}/dM$  term which is proportional to  $M^2$  for small masses whereas the  $dn/dM_{init}$  term is nearly constant. As shown in the next section, the antiproton emission is governed by PBHs with masses below  $10^{14} \text{ g}$ . The results derived are therefore independent of the details of the formation mechanism.

Nevertheless, even if it is not fully relevant for the upper limit derived in this paper, it must be reminded that this formation mechanism is not the only possible one. Critical phenomena have been shown to play a role in gravitational collapses leading to black holes (Choptuik 1993). For some parameter families of field configurations with controlling parameter  $p$ , the black hole masses scale as  $(p - p_c)^{\gamma_s}$  above the critical parameter  $p_c$  with a universal exponent  $\gamma_s \approx 0.37$ . The possible resulting type-II PBHs (Niemeyer & Jedamzik 1999) can exhibit a very different mass spectrum than the previous ones (hereafter referred to as type-I PBHs) because the scaling relation does not require the formation mass to be of order the horizon mass anymore.

### 3.2.2. Cumulative source before propagation

Fig. 3 gives the antiproton flux after convolution with the PBH mass spectrum before propagation. It is important to notice that each mass interval, between  $10^{10} \text{ g}$  and a few times  $M_*$  contributes to the resulting flux. As it could be expected, PBHs heavier than  $M_*$  nearly do not contribute as both their number density and their temperature is low. On the other hand, only PBHs with very small masses, *i.e.* with very high temperatures, contribute to the high energy tail of the antiproton spectrum. It should be noticed that the only reason why they do not also dominate the low energy part is that the mass

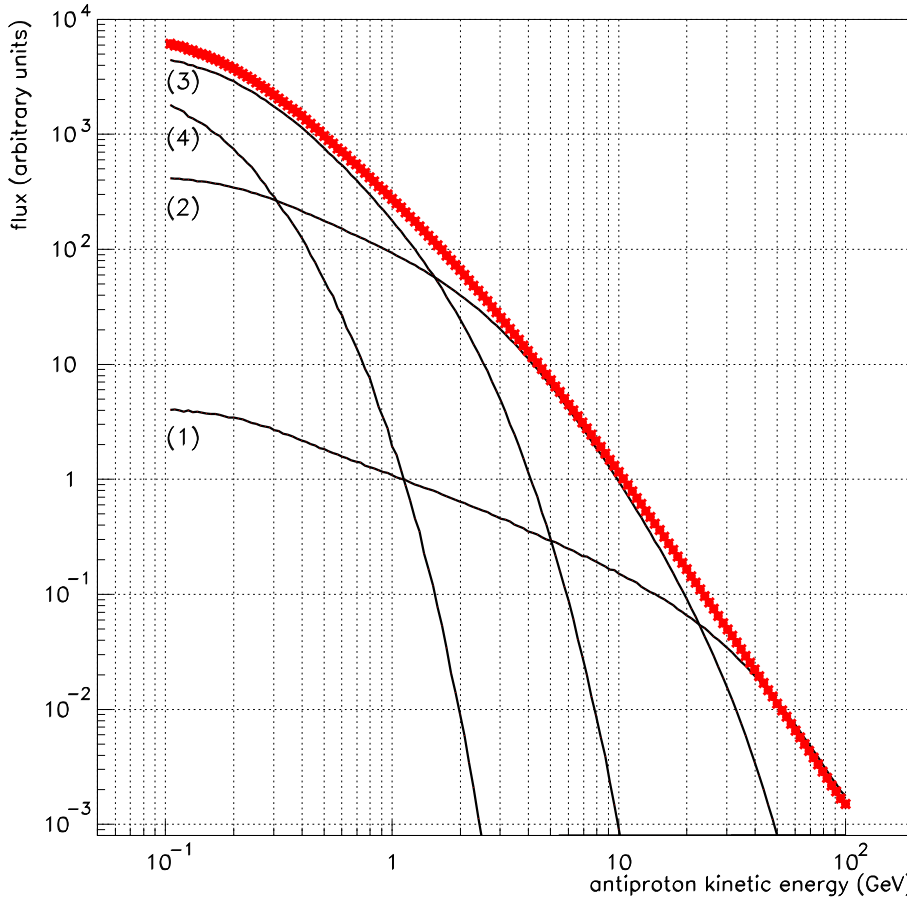


**Fig. 3.** Primary antiproton flux with the standard mass spectrum before propagation (in arbitrary units). Curve (1) is for  $M \in [M_{Pl}, 10^{12} \text{g}]$ , curve (2) is for  $M \in [10^{12} \text{g}, 10^{13} \text{g}]$ , curve (3) is for  $M \in [10^{13} \text{g}, 5 \cdot 10^{13} \text{g}]$ , curve (4) is for  $M > 5 \cdot 10^{13} \text{g}$  and the thick line is the full spectrum.

spectrum behaves like  $M^2$  below  $M_*$ . In a Friedman universe without inflation, this important feature would make the accurate choice of the mass spectrum lower bound  $M_{min}$  irrelevant (as long as it remains much smaller than  $M_*$ ), due to the very small number density of black holes in this mass region.

Fig. 4 shows how inflation modifies the *standard* mass spectrum. The reheating temperature used herafter is nothing else than a way of taking into account a cutoff in the mass spectrum due to the rather large horizon size after inflation. There is nearly no constraint, neither on the theoretical side nor on the observational one, on this reheating temperature. A reliable lower limit can only be imposed by phenomenological arguments around the nucleosynthesis values, *i.e.* in the MeV range (Giudice *et al.* 2001). On the other hand, upper limits, taking into account the full spectrum of inflaton decay products in the thermalization process, are close to  $10^{12}$  GeV (McDonald, 2000). The main point

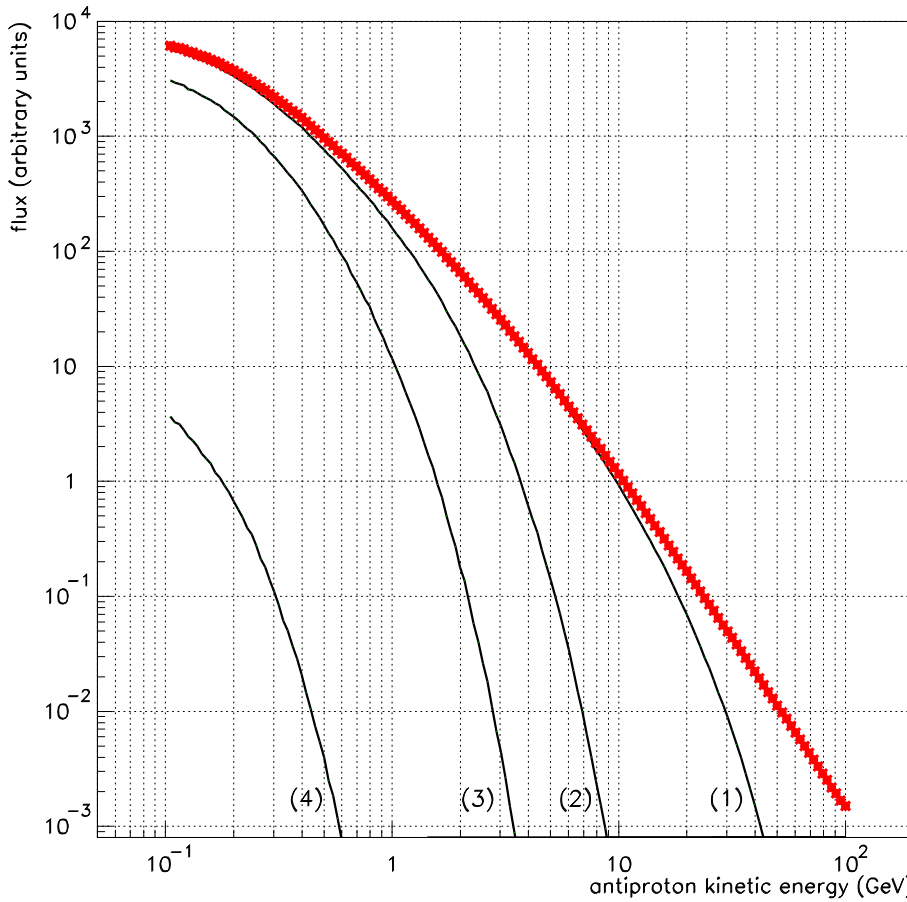


**Fig. 4.** Primary antiproton flux with the standard mass spectrum before propagation (in arbitrary units) with different reheating temperatures. Curve (1) is for  $T_{RH} = 3 \cdot 10^9$  GeV, curve (2) is for  $T_{RH} = 10^9$  GeV, curve (3) is for  $T_{RH} = 6 \cdot 10^8$  GeV, curve (4) is for  $T_{RH} = 3 \cdot 10^8$  GeV and the thick line is the spectrum without any cutoff.

for the antiproton emission study is that there is clearly a critical reheating temperature,  $T_{RH}^c \approx 10^9$  GeV. If  $T_{RH} > T_{RH}^c$ , the *standard* mass spectrum today is nearly not modified by the finite horizon size after inflation, whereas if  $T_{RH} < T_{RH}^c$ , the minimal mass becomes so large that the emission is strongly reduced. It is important to notice, first, that a rather high value of  $T_{RH}^c$  makes the existence of PBHs evaporating now into antiprotons quite unlikely, second, that the flux is varying very fast with  $T_{RH}$  around  $T_{RH}^c$ . One order of magnitude below  $T_{RH}^c$ , the integrated emission is so small that no detection seems possible, while one order above  $T_{RH}^c$ , the flux is not changed up to 100 GeV.

It should also be mentioned that above some critical temperature, the emitted Hawking radiation could interact with itself and form a nearly thermal photosphere (Heckler 1997). This idea was numerically studied (Cline *et al.* 1999) with the full

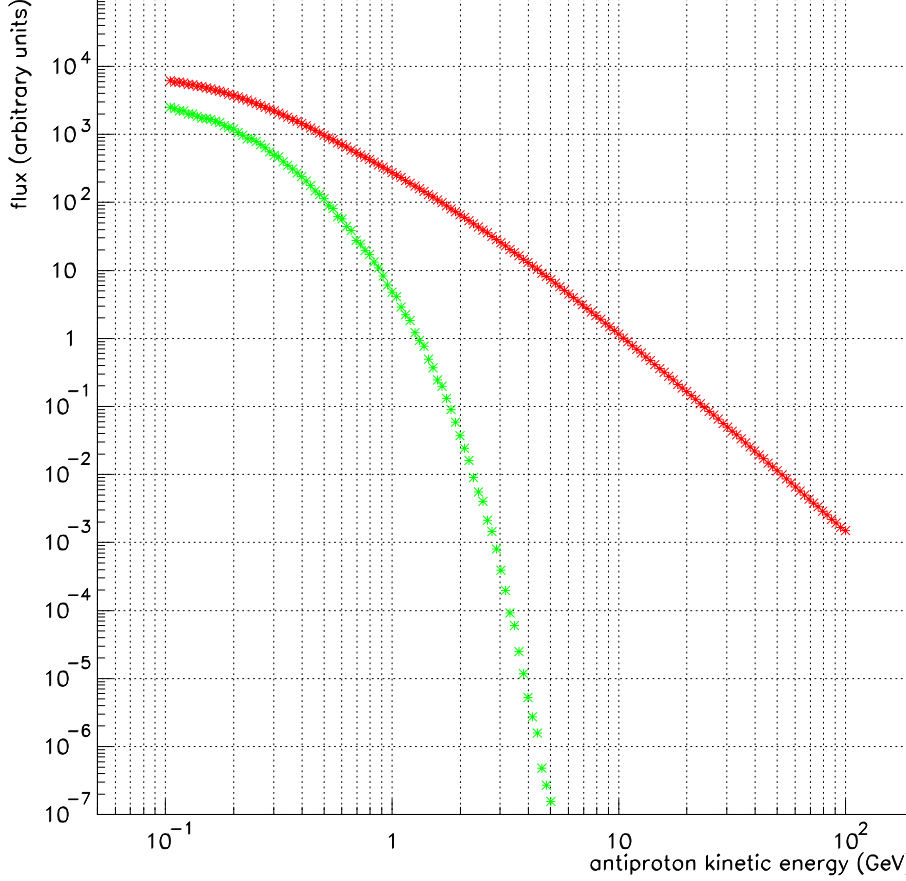


**Fig. 5.** Primary antiproton flux with the standard mass spectrum. The higher points correspond to the pure Hawking spectrum and the lower points to the modified law with a QCD halo.

Boltzmann equation for the particle distribution and the Hawking law as a boundary condition at horizon. For the antiproton emission, the relevant process is the formation of a quark-gluon plasma which induces energy losses before hadronization. We have taken into account this possible effect using the spectrum given by Cline *et al.* (1999)

$$\frac{d^2N}{dEdt} \propto \exp(-E/T_0)$$

where  $T_0 \approx 300$  MeV normalized to the accurately computed Hawking spectrum so that particle production factor  $P(T)$  (*i.e.* the number of particles created in the QCD halo per emitted particle) fulfills

$$P(T) \approx 8.6 \frac{T}{(1\text{GeV})}.$$

The resulting effect, dramatically reducing the evaluated flux, is shown in Fig. 5.

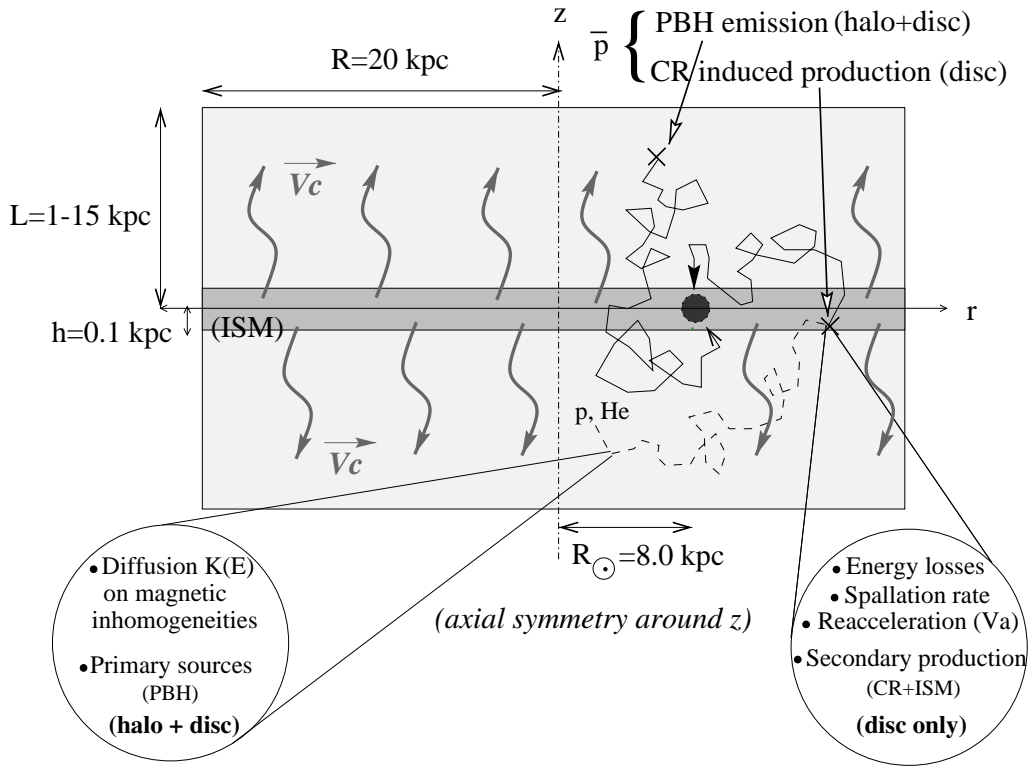


**Fig. 6.** Schematic view of the axi-symmetric diffusion model. Secondary antiproton sources originate from CR/ISM interaction in the disc only (see section 4.1.1); primary sources are also distributed in the dark halo which extends far beyond the diffusion halo (see sections 4.1.2 and 3.1). In the latter case, only sources embedded in the diffusion halo contribute to the signal (see section 4.3).

#### 4. Propagation model

The propagation of cosmic rays throughout the Galaxy is described with a two-zone effective diffusion model which has been thoroughly discussed elsewhere (Maurin *et al.* 2001 - hereafter Paper I, Donato *et al.* 2001a - hereafter Paper II). We repeat here the main features of this diffusion model for the sake of completeness but we refer the reader to the above-mentioned papers for further details and justifications.

The Milky-Way is pictured as a thin gaseous disc with radius  $R = 20$  kpc and thickness  $2h = 200$  pc (see figure 6) where charged nuclei are accelerated and destroyed by collisions on the interstellar gas, yielding secondary cosmic rays. That thin ridge is sandwiched between two thick confinement layers of height  $L$ , called *diffusion halo*. The effective diffusion of cosmic rays throughout the galactic magnetic fields occurs uniformly within the disc and halo with the same strength. Furthermore, we consider here a constant convective wind  $V_c$  in the  $z$  direction. The associated adiabatic losses along with ionization losses and reacceleration take place in the disc only. This model takes into account the minimal known physical processes thought to be present during the

propagation: Galactic wind  $V_c$  has already been mentioned; the efficiency of diffusive reacceleration depends on the Alfvénic velocity  $V_a$ ; spatial diffusion is an energy dependent phenomenon, and the diffusion coefficient may be expressed as  $K(E) = K_0 \beta \times \mathcal{R}^\delta$  where  $\mathcal{R}$  stands for rigidity and  $K_0$  and  $\delta$  are two parameters of the model. The five parameters of this diffusion model are  $K_0$ ,  $\delta$ ,  $L$ ,  $V_c$  and  $V_a$ . Specific treatment related to  $\bar{p}$  interactions (elastic scattering, inelastic destruction) can also be found in Paper II. We now focus on the equilibrium propagation solution for both primaries (PBH evaporation, SUSY annihilation,...) and secondaries (cosmic ray induced) antiprotons.

#### 4.1. Solution of the diffusion equation for antiprotons

The antiproton density  $N^{\bar{p}}$  is related to the antiproton flux through

$$\Phi_{\bar{p}}(r, z, E) = \frac{1}{4\pi} v_{\bar{p}}(E) N^{\bar{p}}(r, z, E) . \quad (4)$$

When energetic losses and gains are discarded, the density  $N^{\bar{p}}$  satisfies the relation (see Paper II for details)

$$2h\delta(z) q^{sec}(r, 0, E) = 2h\delta(z) \Gamma_{\bar{p}}^{ine} N^{\bar{p}}(r, 0, E) + \left\{ V_c \frac{\partial}{\partial z} - K \left( \frac{\partial^2}{\partial z^2} + \frac{1}{r} \frac{\partial}{\partial r} \left( r \frac{\partial}{\partial r} \right) \right) \right\} N^{\bar{p}}(r, z, E) , \quad (5)$$

as long as steady state holds. Nuclear reactions, convection and diffusion have been included.

##### 4.1.1. Secondary contribution

Antiproton cosmic rays have been detected, and most of them were probably secondaries, *i.e.* they were produced by nuclear reactions of a proton or He cosmic ray (CR) nucleus impinging on interstellar (ISM) hydrogen or helium atoms at rest. Due to the cylindrical geometry of the problem, it is easier to extract solutions performing Bessel expansions of all quantities over the orthogonal set of Bessel functions  $J_0(\zeta_i r)$  ( $\zeta_i$  stands for the  $i$ th zero of  $J_0$  and  $i = 1 \dots \infty$ ). The antiproton density and the secondary source term respectively read

$$N^{\bar{p}}(r, z, E) = \sum_{i=1}^{\infty} N_i^{\bar{p}}(z, E) J_0\left(\zeta_i \frac{r}{R}\right) , \quad (6)$$

$$q^{sec}(r, 0, E) = \sum_{i=1}^{\infty} q_i^{sec}(E) J_0\left(\zeta_i \frac{r}{R}\right) , \quad (7)$$

Spallations occur only in the disc, so that the source term  $q^{sec}(r, 0, E)$  (and so does  $q_i^{sec}(E)$ ) depends on the H and He CR fluxes at  $z = 0$ , which are well measured, on the hydrogen and helium densities of the interstellar medium, and on the spallation

cross-sections (see Paper II – sections 3,4 and Appendix – for details). The solution of equation (5) may be written as

$$N_i^{\bar{p}, sec}(z, E) = \frac{2h}{A_i} q_i^{sec}(E) \times \exp \left\{ \frac{V_c |z|}{2K} \right\} \left\{ \sinh \left\{ \frac{S_i}{2} (L - |z|) \right\} / \sinh \left\{ \frac{S_i}{2} L \right\} \right\} , \quad (8)$$

where the quantities  $S_i$  and  $A_i$  are defined as

$$S_i \equiv \left\{ \frac{V_c^2}{K^2} + 4 \frac{\zeta_i^2}{R^2} \right\}^{1/2} \quad \text{and} \quad A_i(E) \equiv 2h \Gamma_{\bar{p}}^{ine} + V_c + K S_i \coth \left\{ \frac{S_i L}{2} \right\} . \quad (9)$$

#### 4.1.2. Primary sources

The antiproton production by PBH is described by a source term distributed over all the dark matter halo (see section 3.1) – this has not to be confused with the diffusion halo – whose core has a typical size of a few kpc. The solution for a generic source term  $q^{prim}(r, z, E)$ , is obtained by making the substitution

$$2h \delta(z) q^{sec}(r, 0, E) \longleftrightarrow q^{prim}(r, z, E) \quad (10)$$

in equation (5). The Bessel expansion of this term now reads

$$q^{prim}(r, z, E) = \sum_{i=1}^{\infty} q_i^{prim}(z, E) J_0 \left( \zeta_i \frac{r}{R} \right) , \quad (11)$$

with (introducing  $\rho \equiv r/R$ )

$$q_i^{prim}(z, E) = \frac{2}{J_1^2(\zeta_i)} \int_0^1 \rho q^{prim}(\rho, z, E) J_0(\zeta_i \rho) d\rho \quad (12)$$

The procedure to find the solutions of equation 5 is standard (see Paper I, Paper II and references therein). First, we Bessel expand this equation into

$$K \left[ \frac{d^2}{dz^2} - \frac{V_c}{K} \frac{d}{dz} - \frac{\zeta_i^2}{R^2} \right] N_i^{\bar{p}}(z, E) = -q_i^{prim}(z, E) + 2h \delta(z) N_i^{\bar{p}}(0, E) \Gamma_{\bar{p}}^{ine} \quad (13)$$

Then, we find a solution in the halo ( $z \geq h$ ), use the boundary condition  $N_i^{\bar{p}}(z = L) = 0$ , and finally assume continuity between disc and halo. The equation to be solved in the halo is

$$K \left[ \frac{d^2}{dz^2} - \frac{V_c}{K} \frac{d}{dz} - \frac{\zeta_i^2}{R^2} \right] N_i^{\bar{p}, prim}(z) = -q_i^{prim}(z) \quad (14)$$

It can be transformed in a set of two first order differential equations by the factorization

$$\left[ \frac{d^2}{dz^2} - \alpha \frac{d}{dz} - \beta \right] \equiv \left[ \frac{d}{dz} + \left( -\alpha + \sqrt{\frac{\alpha^2}{4} + \beta^2} \right) \right] \left[ \frac{d}{dz} + \left( -\alpha - \sqrt{\frac{\alpha^2}{4} + \beta^2} \right) \right] \quad (15)$$

After some algebra, we obtain

$$N_i^{\bar{p}, prim}(z) = \exp \left( \frac{V_c (|z| - L)}{2K} \right) \frac{y_i(L)}{A_i \sinh(S_i L / 2)} \left[ \cosh(S_i z / 2) + \frac{(V_c + 2h \Gamma_{\bar{p}}^{ine})}{K S_i A_i} \sinh(S_i z / 2) \right] - \frac{y_i(z)}{K S_i} \quad (16)$$

where

$$y_i(z) = 2 \int_0^z \exp \left( \frac{V_c}{2K} (z - z') \right) \sinh \left( \frac{S_i}{2} (z - z') \right) q_i^{prim}(z') dz' \quad (17)$$

In particular, at  $z = 0$  where fluxes are measured, we have

$$N_i^{\bar{p}, \text{prim}}(0) = \exp\left(\frac{-V_c L}{2K}\right) \frac{y_i(L)}{A_i \sinh(S_i L/2)} \quad (18)$$

or equivalently (this is the form obtained when the problem is solved by the means of Green functions)

$$N_i^{\bar{p}, \text{prim}}(0) = \exp\left(\frac{-V_c L}{2K}\right) \frac{1}{A_i \sinh(S_i L/2)} \left\{ -\mathcal{Q}_i(L) + \exp\left(\frac{S_i L}{2} + \frac{V_c L}{2K}\right) \mathcal{Q}_i(0) \right\} \quad (19)$$

with

$$\mathcal{Q}_i(z) = \int_0^L \exp\left(\frac{V_c}{2K}(z - z') - \frac{S_i}{2}|z - z'|\right) q_i^{\text{prim}}(z') dz' \quad (20)$$

The careful reader could check that with a secondary source term  $2 h \delta(z) q^{\text{sec}}(r, 0, E)$ , expression (8) is recovered.

#### 4.1.3. General solution: primaries, secondaries and energy losses and gains

This is not the final word, as the antiproton spectrum is affected by energy losses when the  $\bar{p}$  interact with the galactic interstellar matter and by energy gains when reacceleration occurs. These energy changes are described by the integro-differential equation

$$A_i N_i^{\bar{p}} + 2 h \partial_E \{ b_{\text{loss}}^{\bar{p}}(E) N_i^{\bar{p}} - K_{EE}^{\bar{p}}(E) \partial_E N_i^{\bar{p}} \} = 2 h \left\{ q_i^{\text{prim}}(E) + q_i^{\text{sec}}(E) + q_i^{\text{ter}}(E) \right\} \quad (21)$$

We added a source term  $q_i^{\text{ter}}(E)$ , leading to the so-called tertiary component. It corresponds to inelastic but non-annihilating reactions of  $\bar{p}$  on interstellar matter, as discussed in Paper II. The resolution of this equation proceeds as described in Appendix (A.2), (A.3) and Appendix (B) of Paper II, to which we refer for further details. The total antiproton flux is finally given by

$$N^{\bar{p}, \text{tot}}(R_\odot, 0, E) = \sum_{i=1}^{\infty} \left( N_i^{\bar{p}, \text{sec}}(0, E) + N_i^{\bar{p}, \text{prim}}(0, E) \right) J_0\left(\zeta_i \frac{R_\odot}{R}\right) \quad (22)$$

where  $N_i^{\bar{p}, \text{sec}}(0, E)$  and  $N_i^{\bar{p}, \text{prim}}(0, E)$  are given by formulæ (8), (17) and (18). We emphasize that the code (and thus numerical procedures) used in this study is exactly the same as the one we used in our previous analysis (Paper I and II), with the new primary source term described above.

#### 4.2. Parameter space allowed by stable cosmic ray studies and used to derive antiproton spectrum

Actually, a confident range for the five parameters of our diffusion model has been obtained by the analysis of charged stable cosmic ray nuclei data (see Paper I). The selected parameters have been employed in Paper II to study the secondary antiproton flux, and are used again in this analysis (for specific considerations about the Alfvén velocity, see section 5.2 of Paper II). In principle, this range could be further reduced using more

precise data or considering different sorts of cosmic rays. For the particular case of  $\beta$  radioactive nuclei, Donato *et al.* 2001b showed that with existing data no definitive and strict conclusions can so far be drawn. We thus have chosen a conservative attitude and we do not apply any cut in our initial sets of parameters (which can be seen in figures 7 and 8 of Paper I).

#### 4.3. Sources located outside the diffusive halo

As previously noticed, the dark halo extends far beyond the diffusion halo whereas its core is grossly embedded within  $L$ . We can wonder if the external sources not comprised in the diffusive halo significantly contribute to the amount of  $\bar{p}$  reaching Earth. By definition, diffusion is much less efficient outside of the diffusive halo, so that antiprotons coming from these outer sources propagate almost freely, until they reach the diffusion box boundary. At this point, they start to interact with the diffusive medium and after travelling a distance of the order of the mean free path, their propagation becomes diffusive. Thus, the flux of incoming antiprotons gives rise to three thin sources located at the surfaces  $\sigma_1$ ,  $\sigma_2$  and  $\sigma_3$  (see figure 4.3.1), the first with a  $z$  distribution  $\eta(z)$  which has non-zero values only for  $z \sim L$  (the upper boundary of the diffusive volume), the second with a  $r$  distribution  $\eta(r)$  which has non-zero values only for  $r \sim R$  (the side boundary) and the third located at  $z \approx -L$  (the lower boundary).

##### 4.3.1. Solar density of antiprotons coming from external sources

Let us focus first on the top and bottom surfaces  $\sigma_1$  and  $\sigma_3$  located at  $z \sim L$ . As expression (18) was obtained for a symmetrical source term, the corresponding external source term can be directly written as

$$q^{ext}(r, z) = \mathcal{F}^{inc}(r)\eta(L - z) \quad \text{with} \quad \int \eta(z)dz = 1$$

where  $\eta(z)dz$  is the probability for an incoming nucleus to interact with the diffusive medium in the layer comprised between distances  $z$  and  $z + dz$  from the boundary, and  $\mathcal{F}^{inc}(r)$  is the antiproton flux coming from outside the diffusive halo. The function  $\eta(z)$  is expressed in  $\text{kpc}^{-1}$ . Using the fact that the surface source is located around small values of  $u \equiv L - z$ , insertion of the above relation in formula (17) gives

$$y_i^{ext}(L) \approx 2\mathcal{F}_i^{inc} \frac{S_i}{2} \int u\eta(u)du = \mathcal{F}_i^{inc}(r)S_i\bar{u}$$

where  $\mathcal{F}_i^{inc}$  is the Bessel transform of  $\mathcal{F}^{inc}(r)$  and where the mean free path  $\bar{u} = \int u\eta(u)du$  has been introduced, so that (18) becomes

$$N_i^{ext}(0) = \exp\left(\frac{-V_c L}{2K}\right) \frac{\mathcal{F}_i^{inc} S_i \bar{u}}{A_i \sinh(S_i L/2)} \quad (23)$$

Before turning to the computation of the incoming flux  $\mathcal{F}^{inc}(r)$  at the box boundary, we can make a remark about the above expression. If galactic wind and spallations are neglected, it can be simplified into

$$N_i^{ext}(0) \approx \frac{\mathcal{F}_i^{inc} \bar{u}}{K \cosh(\zeta_i L/R)}$$

It occurs that the diffusion coefficient  $K$  and the mean free path  $\bar{u}$  are related in a way that depends on the microscopic details of the diffusion process. For hard spheres diffusion,  $\bar{u} = 3K/v$  so that

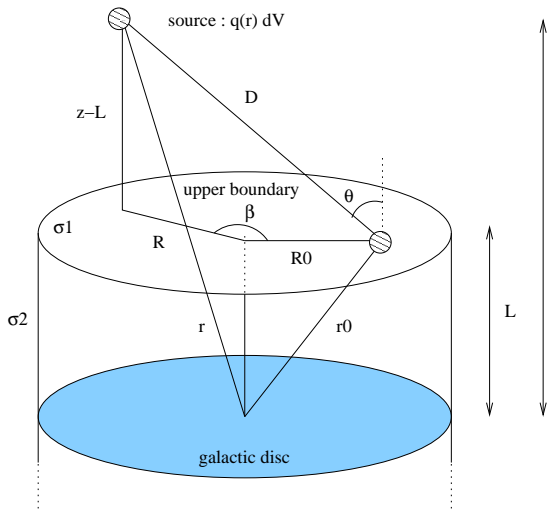
$$N_i^{ext}(0) \approx \frac{3\mathcal{F}_i^{inc}}{v \cosh(\zeta_i L/R)}$$

The physical interpretation of this expression is interesting: for low Bessel indices  $i$ , *i.e.* for large spatial scales, the  $\cosh(\zeta_i L/R)$  term is close to unity and the Bessel terms in the disk density are proportional to those in the source term. For large Bessel indices  $i$ , *i.e.* for small spatial scales, the Bessel terms are exponentially lowered in the disk density compared to the source term. The small scale variations of the source are filtered out by the diffusion process. This filtering is more efficient for large values of the diffusion zone height  $L$ .

In the following, we show the results for the full expression

$$N_i^{ext}(0) = \exp\left(\frac{-V_c L}{2K}\right) \frac{\mathcal{F}_i^{inc} S_i 3K}{\beta c A_i \sinh(S_i L/2)} \quad (24)$$

where the hard sphere expression has been used for  $\bar{u}$ .



#### 4.3.2. Computation of the incoming flux $\mathcal{F}^{inc}(r)$ from external sources

The flux of nuclei reaching the surface from a source located outside the diffusive halo is

$$d\mathcal{F}^{inc} = \cos \theta \frac{q_{PBH}(\mathbf{r}) dV}{4\pi D^2}$$

with  $\cos \theta = (z - L)/D$ , so that

$$\mathcal{F}^{inc}(r) = \iiint \frac{(z - L)q_{PBH}(\mathbf{r})}{4\pi D^3} R d\beta dR dz$$

Using the fact that  $\mathbf{D} = \mathbf{r} - \mathbf{r}_0$ , we have

$$D^2 = (z - L)^2 + R^2 + R_0^2 - 2RR_0 \cos \beta$$

The integration over the angular coordinate  $\beta$  is performed using the property (see Gradshteyn 1980)

$$\int_0^\pi \frac{d\beta}{(a - b \cos \beta)^{3/2}} = \frac{2\mathbf{E}(x)}{(a - b)\sqrt{a + b}}$$

where  $\mathbf{E}$  is the elliptic function (denoted  $R_F$  in Numerical Recipes, 1992) and where  $x \equiv \sqrt{2b/(a + b)}$ . Finally, we can write

$$\mathcal{F}^{inc}(r) = \int_{R=0}^{\infty} \int_{z=L}^{\infty} \frac{q_{PBH}(\mathbf{r})}{4\pi} \frac{2\mathbf{E}(x)(z - L)R dR dz}{((z - L)^2 + (R - R_0)^2)\sqrt{(z - L)^2 + (R + R_0)^2}}$$

This quantity is then numerically computed and Bessel-transformed to be incorporated in eq. (24).

#### 4.3.3. Conclusion: the external contribution is negligible

The contribution of these external sources is shown in table 1 for  $L = 1$  kpc (the lowest value we allowed) and  $L = 5$  kpc, with or without galactic wind. It is larger for lower halo heights  $L$ , but it is always less than  $10^{-4}$  and it can be safely neglected.

**Table 1.** Fraction  $N_{ext}/N_{tot}$  of the antiproton density in the solar neighbourhood due to the external primary sources, for the PBH density profiles discussed in the text. The relevant cross-sections for antiproton spallations have been considered in the  $A_i$  term, and a kinetic energy of 1 GeV has been assumed. The results are not very sensitive to this particular energy value.

density profile	$V_c = 0$ km/s		$V_c = 10$ km/s	
	$L = 1$ kpc	$L = 5$ kpc	$L = 1$ kpc	$L = 5$ kpc
Moore	$1.7 \times 10^{-4}$	$4.9 \times 10^{-6}$	$4.9 \times 10^{-6}$	$4.0 \times 10^{-15}$
NFW	$1.8 \times 10^{-4}$	$5.4 \times 10^{-6}$	$5.4 \times 10^{-6}$	$4.3 \times 10^{-15}$
Modified isothermal	$2.5 \times 10^{-4}$	$9.3 \times 10^{-6}$	$1.5 \times 10^{-5}$	$7.0 \times 10^{-15}$
Isothermal	$1.7 \times 10^{-4}$	$4.3 \times 10^{-6}$	$1.0 \times 10^{-5}$	$3.6 \times 10^{-15}$

Similar results apply to the side boundary  $\sigma_2$  which is about  $R_{gal} - R_\odot \sim 12$  kpc away. Roughly, the contribution is the same order of magnitude than would be obtained with a thin source  $\sigma_1$  located at  $z = 12$  kpc, which can be neglected as discussed above.

Note also that we present here only two combinations of  $V_c$  and  $L$  to derive the surface contribution, but all the good sets of propagation parameters used throughout this paper

(and also in Paper I and Paper II) point toward the same values, which are not larger than those derived in table 1. We can thus conclude that primary surface contributions are negligible in all cases.

## 5. Top of atmosphere spectrum

### 5.1. Summary of the inputs

For the numerical results presented here, we have considered a source term (see section 3.1)

$$q^{prim}(r, z, E) = \rho_{\odot}^{PBH} \left( \frac{R_c^2 + R_{\odot}^2}{R_c^2 + r^2 + z^2/f^2} \right) \times Q^{PBH}(E)$$

where  $Q^{PBH}(E)$  was shown in figures (3), (4) and (5) for various assumptions.

The spatial distribution corresponds to the isothermal case with a core radius  $R_c = 3$  kpc (the results are modified only by a few percents if  $R_c$  is varied between 2 and 6 kpc) and  $R_{\odot} = 8$  kpc. The possible flatness  $f$  of this halo has also been checked to be irrelevant. Finally the Moore or NFW halos do not need to be directly computed for this study as they only increase the total PBH density inside the diffusion volume for a given local density: as a result the flux is higher and the more conservative upper limit is given by the isothermal case.

The (5.1) primary source term is injected in eq. 17 and 18, then added to the standard secondary contribution (eq. 8), and propagated (eq. 21) for a given set of parameters (see section 4.2). Once this interstellar flux has been calculated, it must be corrected for the effects of the solar wind, in order to be compared with the top of atmosphere observations. We have obtained the TOA fluxes following the usual force field approximation (see Donato *et al.* 2000 and references therein). Since we will compare our predictions with data taken during a period of minimal solar activity, we have fixed the solar modulation parameter to  $\phi = 500$  MV.

To summarize, the whole calculation is iterated for many  $Q^{PBH}(E)$  input spectra, and various values of the propagation parameters  $V_c$ ,  $L$ ,  $K_0$ ,  $V_a$ ,  $\delta$ . Once the derived flux is modulated, its comparison to data gives constraints on the local PBH density  $\rho_{\odot}^{PBH}$ .

### 5.2. Features of the propagated PBH spectrum

Fig. 7 shows the top of atmosphere antiproton flux resulting from the *standard* mass spectrum without any inflation cutoff ( $T_{RH} > T_{RH}^c$ ) for a local density  $\rho_{\odot}^{PBH} = 10^{-32}$  g cm<sup>-3</sup>. The two curves correspond to the extreme astrophysical models considered as acceptable in the extensive study of nuclei below  $Z = 30$  (paper I). We can notice that uncertainties due to astrophysical parameters are very important on the primary propagated  $\bar{p}$  flux. The degeneracy in the diffusion parameters that one can observe for stable nuclei – and also for secondary antiprotons (see figure 7 of Paper II) – is broken down for PBH  $\bar{p}$ 's.

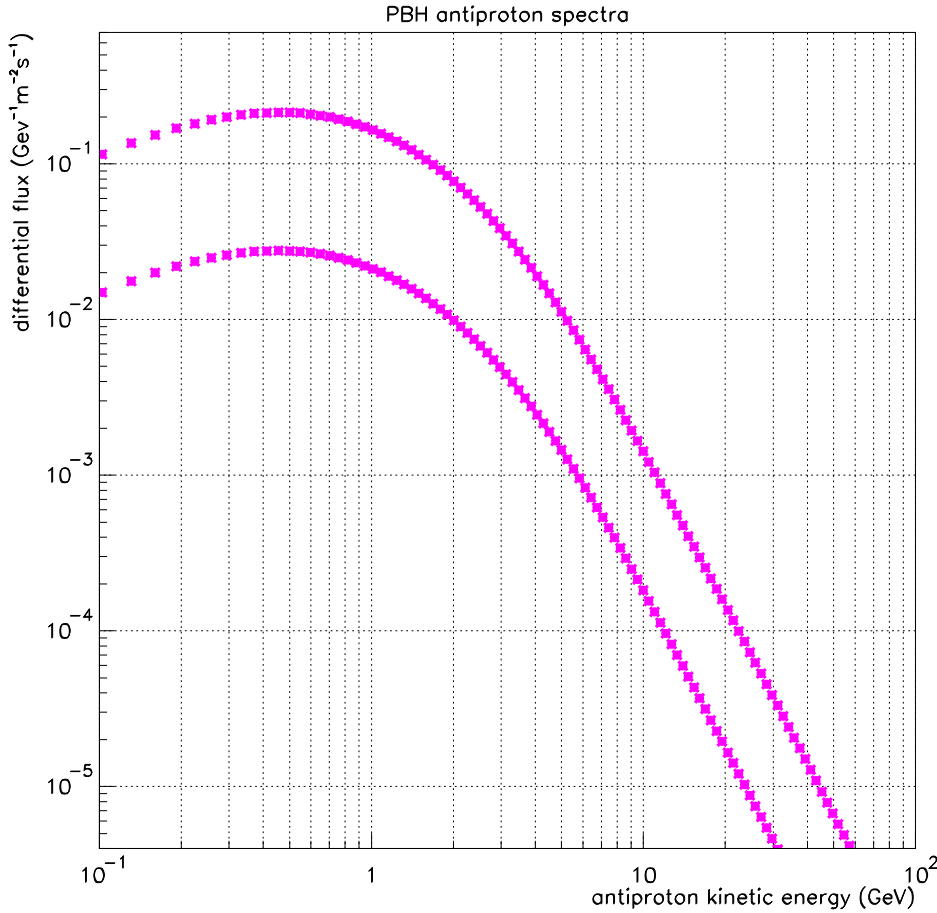


**Fig. 7.** TOA primary antiproton flux with the standard mass spectrum after propagation for  $\rho_{\odot}^{PBH} = 10^{-32}$  g cm<sup>-3</sup> and extreme astrophysical models.

This can be easily understood: secondary  $\bar{p}$  and CR nuclei are created by spallations in the galactic disc, so that all the sets of diffusion parameters that make the primaries cross the same grammage ( $\sim 20$  g cm<sup>-2</sup>) give the same secondary flux. The simplest diffusion models (no reacceleration, no galactic wind – see for example Webber *et al.* 1992) predict that the only relevant parameter is then  $K_0/L$ . On the other hand, primary antiprotons sources are located in the dark matter halo, and their flux is very sensitive to the total quantity of sources contained in the diffusion halo, *i.e.* to  $L$ . This explains the scatter of about one order of magnitude in predicted fluxes that are shown in Fig. 7 for a given local density.

### 5.3. Comparison with previous works

In our models, all sets of parameters compatible with B/C have been retained. In particular, a wide range of values for  $L$  is allowed ( $L \geq 1$  kpc) and each  $L$  is correlated with

the other parameters (for an analytical relation between parameters, see Taillet & al in preparation). Indeed, in Paper I we decided to limit the upper value for  $L$  to 15 kpc. To a certain extent, this choice was arbitrary, but somehow motivated by physical arguments (see for example Beuermann *et al.* 1985 and Han *et al.* 1997 for direct observation of radio halos in galaxies, showing that  $L$  is a few kpc, and Dogiel 1991 for a compilation of evidences).

To our knowledge, the most complete studies about primary PBH antiprotons are those by Mitsui *et al.* (1996) and Maki *et al.* (1996), in which the authors use roughly adjusted values for diffusion parameters and restrict their analysis to two cases,  $L = 2$  kpc and  $L = 4$  kpc. This is somewhat a crude estimation of what we know (or don't know) about  $L$ . Moreover, in their models, neither galactic wind nor reacceleration is considered. The second point should not be very important (see Paper II) whereas the first point has a crucial impact on the detected antiproton flux. As demonstrated by Taillet *et al.* (in preparation), the probability that a primary  $\bar{p}$  detected near Earth has been created at height  $z$  is at least exponentially decreased by the presence of a Galactic wind: setting  $V_c = 0$  may overestimate the number of primary  $\bar{p}$  reaching Earth.

Effects of propagation parameters on primaries are qualitatively discussed in Bergström *et al.* (1999) for the case of SUSY primary antiprotons. At variance with all previous works on the subject, our treatment allows a systematic and quantitative estimation of these uncertainties, as the allowed range of propagation parameters is known from complementary cosmic ray analysis.

## 6. Upper limit on the PBH density

### 6.1. Method

Of course, the previously mentioned uncertainties will clearly weaken the usual upper limits on PBH density derived from antiprotons. To derive a reliable upper limit, and to account for asymmetric error bars in data, we define a generalized  $\chi^2$  as

$$\chi^2 = \sum_i \frac{(\Phi^{th}(Q_i) - \Phi_i^{exp})^2}{(\sigma_i^{exp+} + \sigma_i^{th+}(Q_i))^2} \Theta(\Phi^{th}(Q_i) - \Phi_i^{exp}) + \sum_i \frac{(\Phi^{th}(Q_i) - \Phi_i^{exp})^2}{(\sigma_i^{exp-} + \sigma_i^{th-}(Q_i))^2} \Theta(\Phi_i^{exp} - \Phi^{th}(Q_i)).$$

where  $\sigma^{th+}$  and  $\sigma^{exp+}$  ( $\sigma^{th-}$  and  $\sigma^{exp-}$ ) are the theoretical and experimental positive (negative) uncertainties. Superimposed with BESS(Orito *et al.* 2000, Maeno *et al.* 2000), CAPRICE (CAPRICE Coll. 2001) and AMS data (Alcaraz *et al.* 2001), the full antiproton flux, including the secondary component and the primary component, is shown on Fig. 8 for 20 values of  $\rho_{\odot}^{PBH}$  logarithmically spaced between  $5 \cdot 10^{-35}$  and  $10^{-32} \text{ g cm}^{-3}$ . The *standard* mass spectrum is assumed and one astrophysical model is arbitrarily chosen, roughly corresponding to the average set of free parameters.

The primary fluxes are very sensitive, among all diffusion parameters, to the magnetic halo thickness. Unfortunately, it is widely unknown, and it is not so straightforward to convert this into a sound statistical uncertainty. Instead, we derived an upper limit on the primary flux for each value of the thickness. The theoretical errors included in the  $\chi^2$  function come from nuclear physics and from the astrophysical parameters analysis which were added linearly, in order to remain conservative.

The first ones are mostly due to  $p + He \rightarrow \bar{p} + X$  and  $He + He \rightarrow \bar{p} + X$  spallation processes of cosmic rays on the interstellar medium : they have been discussed and evaluated with their uncertainties in Paper II. As regards the second ones, values of the astrophysical parameters giving a good fit to B/C can be extracted from paper I once  $L$  is fixed.

Taken at face value, the quoted  $\chi^2$  would imply that these sets of parameters correspond to a very stringent limit. It is probably very haphazard to give such a precise statistical meaning to their  $\chi^2$  values, and we chose to be *very* conservative, by assuming that their limits on the parameters correspond to a 1 sigma limit. Anyway, our final conclusions are not very sensitive to this assumption: were the paper I results be considered as a very stringent limit, the total uncertainty would become dominated by the nuclear errors.

## 6.2. Results

For each value of the magnetic halo thickness, the  $\chi^2$  has been computed as a function of  $\rho_{\odot}^{PBH}$ . Fig. 9 gives its variation for  $L = 3$  kpc. The horizontal lines correspond to 63% and 99% confidence levels. In all this paper the statistical significance of such numbers should be taken with care : they only refer to orders of magnitude. As expected, the  $\chi^2$  value is constant for small PBH densities (only secondaries contribute to the flux) and is monotonically increasing without any minimum : this shows that no PBH (or any other primary source) term is needed to account for the observed antiproton flux.

Fig. 10 gives the upper limits on the local density of PBHs as a function of  $L$  with the *standard* mass spectrum. It is a decreasing function of the halo size because a bigger diffusion region means a higher number of PBHs inside the magnetic zone for a given local density. Between  $L = 1$  and  $L = 15$  kpc (extreme astrophysical values), the 99% confidence level upper limit goes from  $5.3 \cdot 10^{-33} \text{ g cm}^{-3}$  to  $5.1 \cdot 10^{-34} \text{ g cm}^{-3}$ .

Although the chosen constrained quantity is not the same, this limit is clearly weaker than the one obtained by Maki *et al.* (1996). This is mainly due to the much more refined propagation model used here and to the more careful analysis of astrophysical uncertainties.

An important point shown in section (3.2.2) is that we are sensitive only to PBHs with masses between  $10^{12} \text{ g}$  and  $10^{14} \text{ g}$ . The upper limit given here on the total local mass

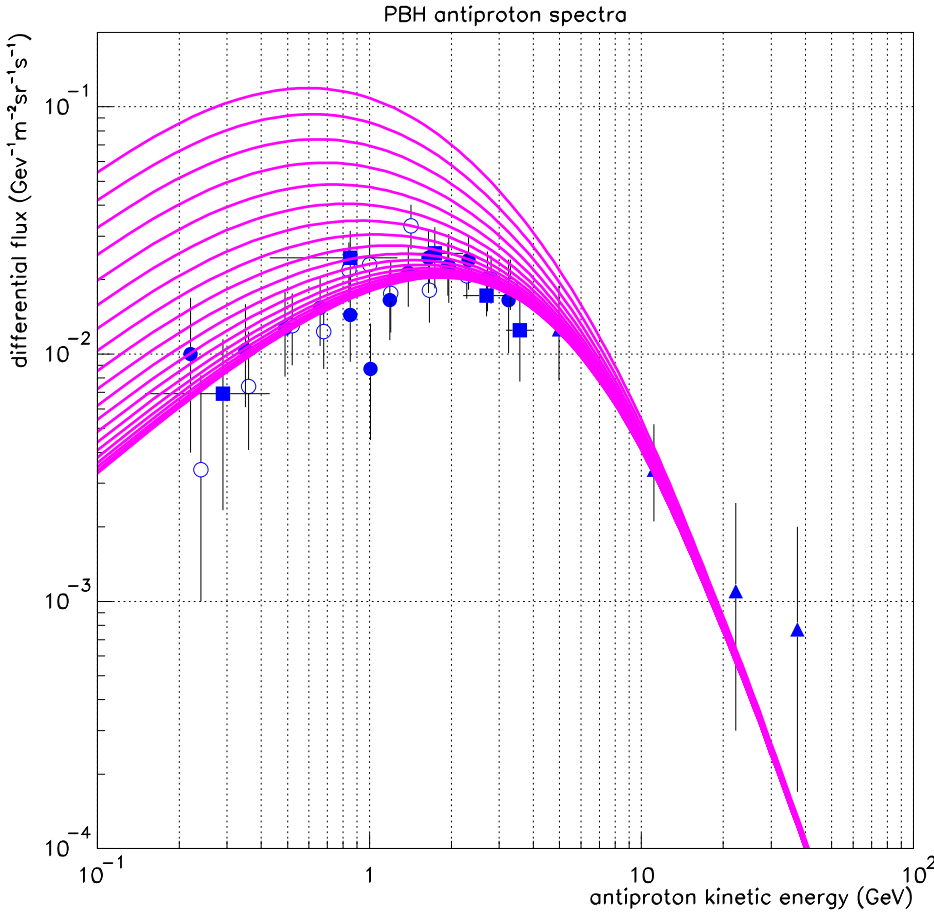


**Fig. 8.** Experimental data from BESS95 (filled circles), BESS98 (circles), CAPRICE (triangles) and AMS (squares) superimposed with mean theoretical PBH spectra for  $\rho_{\odot}^{PBH}$  between  $5 \cdot 10^{-35} \text{ g.cm}^{-3}$  (lower curve) and  $10^{-32} \text{ g cm}^{-3}$  (upper curve).

density of PBHs can therefore be given in a “safer” way as a numerical density of PBHs integrated between  $10^{12} \text{ g}$  and  $10^{14} \text{ g}$ . Although less interesting from the point of view of cosmology, this value has the great interest of being totally model independent as this remains within the “increasing” part of the mass spectrum. The resulting numerical density is  $n_{\odot}^{PBH} = 3.9 \cdot 10^{-51} \text{ cm}^{-3}$  for  $L = 3 \text{ kpc}$ .

If we take into account the possible QCD photosphere (see figure 5) around PBHs whose temperature is greater than  $\Lambda_{QCD}$  the previous upper limit can be substantially weakened. Although the effect is not huge on the low energy tail of the spectrum, it suppresses the multi-GeV emission. The resulting maximal local density, for the “usual”  $L = 3 \text{ kpc}$  halo thickness, is  $\rho_{\odot}^{PBH} < 1.2 \cdot 10^{-32} \text{ g cm}^{-3}$ . In this case, gamma-rays are a much more powerful tool to study PBHs. It should, nevertheless, be emphasized that this model is still controversial. First of all, because the quarks and gluons which are below threshold for pion production seem to be simply ignored, then, because the assumption

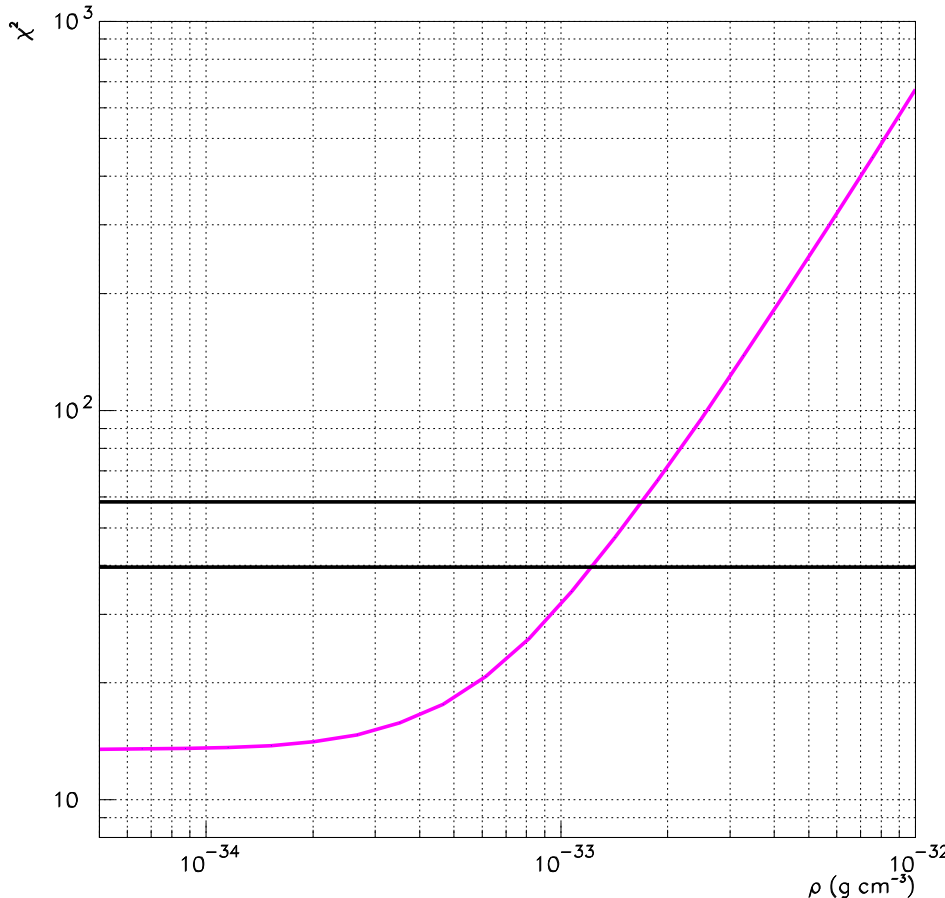


**Fig. 9.**  $\chi^2$  between the experimental data and the theoretical flux as a function of the local density of PBHs for a magnetic halo thickness of 3 kpc. The horizontal lines are 99% and 63% confidence levels.

that the Bremsstrahlung interaction has a range of  $1/m_e$  could be wrong for the hard interactions which would lead to a great overestimation of the photosphere effect (Cline, private communication).

## 7. Discussion and future prospects

Many upper limits on the PBH explosion rate have been derived. A reliable search for short bursts of ultra high-energy gamma radiations from an arbitrary direction have been performed using the CYGNUS air-shower array (Alexandreas *et al.* 1993). No strong one second burst was observed and the resulting upper limit, based on the exhaustive analysis of a very fine binning of the sky, is in the range  $dN_{\odot exp}^{PBH} / dt d^3V \leq 0.9 \cdot 10^6 \text{ year}^{-1} \text{pc}^{-3}$ . Very similar results were derived by the Tibet (Amenomori *et al.* 1995) and the AIROBIC collaborations (Funk *et al.* 1995). TeV gamma-rays have also been used to search for short time-scale coincidence events. The very high-energy gamma-ray bursts detected

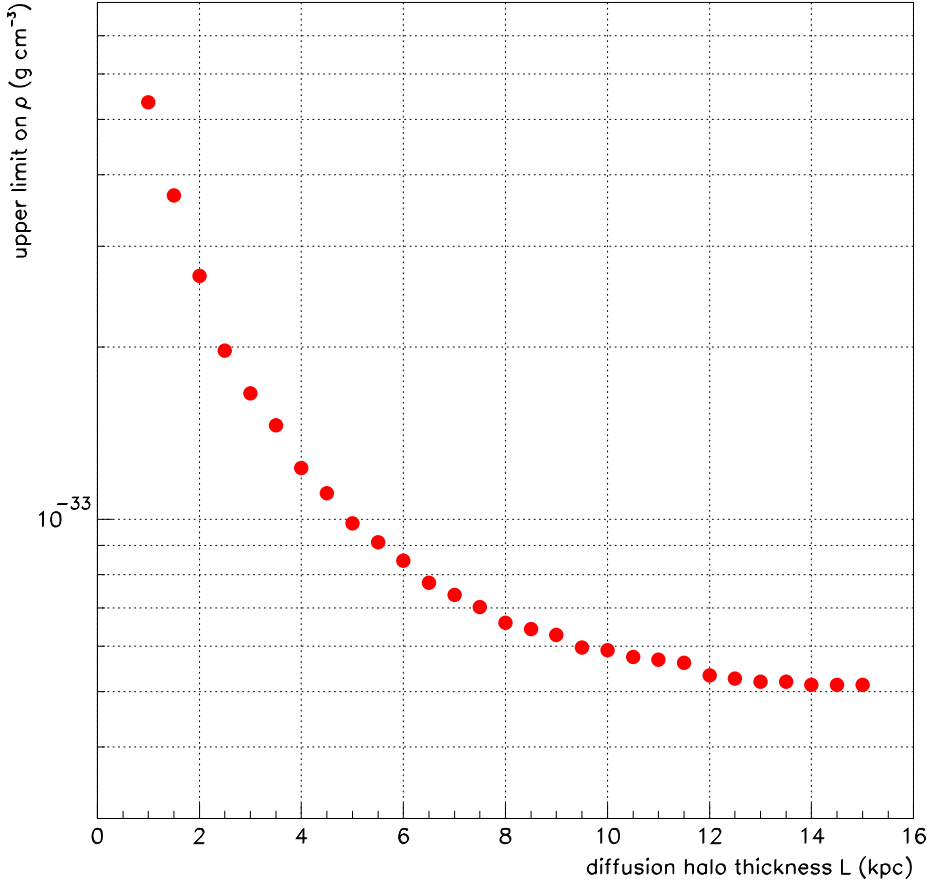


**Fig. 10.** Upper limits on the local density of PBHs as a function of the magnetic halo thickness L.

are compatible with the expected background and the resulting upper limit obtained with 5 years of data (Connaughton 1998) is  $dN_{\odot\text{exp}}^{PBH}/dt d^3V \leq 3 \cdot 10^6 \text{ year}^{-1} \text{ pc}^{-3}$ .

The previously mentioned limit based on antiprotons, from Maki *et al.* (1996), remains far better:  $dN_{\odot\text{exp}}^{PBH}/dt d^3V \leq 2 \cdot 10^{-2} \text{ year}^{-1} \text{ pc}^{-3}$ . We emphasize that this limit is obtained with quite optimistic diffusion models. Moreover, we believe that the explosion rate is not the pertinent variable to use when comparing results from different approaches. Indeed, the thresholds differences between experiments make the meaning of explosion very different. We should keep in mind that the mass spectrum is  $dn/dM \propto M^2$  for small masses and the number of PBHs below the mass corresponding to the threshold of the considered detector is therefore very rapidly varying with the value of this threshold. This is why we prefer to give our upper limit, either as a local mass density, assuming a *standard* mass spectrum,  $\rho_{\odot}^{PBH} < 5.3 \cdot 10^{-33} \text{ g cm}^{-3}$ , either as a number density, totally model independant,  $n_{\odot}^{PBH} < 1.3 \cdot 10^{-50} \text{ cm}^{-3}$  (whatever L). It should be emphasized that astrophysical and nuclear physics uncertainties fundamentally determine the effi-

ciency of this approach. New data on stable nuclei along with a better understanding of diffusion models (see for example Donato et al., in preparation) could allow refinement in propagation to better constrain  $L$ , which is, at least from the propagation point of view, the major source of uncertainties for antiprotons primary evaluations. It is also important to notice that the colour emission treatment could probably be improved. Studying more accurately the colour field confinement and the effects of angular momentum quantization, it has been shown (Golubkov *et al.* 2000) that the meson emission is modified. Those ideas have not yet been applied to baryonic evaporation.

Gamma-rays in the 100 MeV region probably remain the most sensitive probe to look for PBHs (MacGibbon & Carr 1991). Nevertheless, the resulting limit  $\Omega_{PBH} \leq 1.8 \cdot 10^{-8} \approx 1.7 \cdot 10^{-37} \text{ g cm}^{-3}$ , is based on an integration of the signal in time and distance which is much larger than for antiprotons. The energies involved are also associated with a higher mass range. It makes a wide difference in the meaning of the constrained quantity.

Several improvements could be expected for the detection of antimatter from PBHs in the years to come. First, the AMS experiment (Barrau 2001) will allow, between 2004 and 2007, an extremely precise measurement of the antiproton spectrum, with virtually no statistical uncertainties due to the long exposure time and very small systematics thanks to beam calibrations of the detector. In the meanwhile, the BESS (Orito *et al.* 2001) and PAMELA (Straulino *et al.* 2001) experiments should have gathered new high-quality data. The solar modulation effect should be taken into account more precisely to discriminate between primary and secondary antiprotons as the shape of each component will not be affected in the same way. The effect of polarity should also be included (Asaoka *et al.* 2001).

To conclude, the antideuteron signal should be studied as it could be the key-point to distinguish between PBH-induced and SUSY-induced antimatter in cosmic rays. Although the  $\bar{p}$  emission due to the annihilation of supersymmetric dark matter would have nearly the same spectral characteristics than the PBH evaporation signal (a spectrum softer than the secondary component) the antideuteron production should be very different as coalescence scheme usually considered (Chardonnet *et al.* 1997) cannot take place between successive PBH jets.

*Acknowledgements.* The authors would like to thank J.H. Mc Gibbon for very helpful discussions and D. Page for providing the absorption cross-sections.

## References

- Alcaraz, J. *et al.*, the AMS Coll., to be published in Phys. Rep.
- Alexandreas, D. E., Allen, G. E., Berley, D., et al. 1993, Phys. Rev. Lett., 71, 2524
- Alexeyev, S. O., Sazhin, M. V., & Pomazanov, M. V. 2001, Int. J. Mod. Phys. D, 10, 225
- Amenomori, M. *et al.*, 1995, Proc 24th ICRC, Rome, Vol. 2 p112
- Asaoka, Y. *et al.*, 2001, Proceedings of ICRC 2001

Barrau, A. 2000, *Astropart. Phys.*, 12, 269

Barrau, A., & Alexeyev, S. 2001, SF2A meeting proceedings, EDPS Conference Series in *A&A*

Barrau, A. 2001, Proceedings of the Rencontres de Moriond, Very High Energy Phenomena in the Universe, Les Arcs, France (January 20-27, 2001), astro-ph/0106196

Bergström, L., Edsjö, J., & Ullio, P. 1999, *ApJ*, 526, 215

Beuermann, K., Kanbach, G., & Berkhuijsen, E. M. 1985, *A&A*, 153, 17

Bugaev, E. V., & Konishchev, K. V. 2001, preprint astro-ph/0103265

Calcareo-Roldan, C., & Moore, B., 2000, *Phys.Rev. D*62, 123005

Canuto, V., 1978, *MNRAS*, 184, 721

The CAPRICE coll., submitted to *ApJ*, astro-ph/0103513

Carr, B. J., & Hawking, S. W. 1974, *MNRAS*, 168, 399

Carr, B. J. 1975, *ApJ*, 201, 1

Carr, B. J. 2001, Lecture delivered at the Nato Advanced Study Institute. Erice 6th-17th December 2000. Eds. H.J.de Vega, I.Khalatnikov, N.Sanchez

Chardonnet, P., Orloff, J., & Salati, P. 1997, *Phys.Lett. B*, 409, 313

Choptuik, M. W. 1993, *Phys. Rev. Lett.*, 70, 9

Cline, J. M., Mostoslavsky, M., & Servant, G. 1999, *Phys.Rev. D*, 59, 063009

Connaughton, V. 1998, *Astropart. Phys.*, 8, 179

Debattista, V. P., & Sellwood, J.A., 1998, *ApJ*, 493 L5

Debattista, V. P., & Sellwood, J.A., 2000, *ApJ* 543, 704

Dogiel, V. A., 1991, I.A.U. Symposium, 144, 175

Donato, F., Fornengo, N., & Salati, P. 2000, *Phys.Rev. D*, 62, 043003

Donato, F., Maurin, D., Salati, P., et al. 2001a, *ApJ*, 563, 172 *ApJ*, in press (Paper II)

Donato, F., Maurin, D., & Taillet, R. 2001b, accepted in *A&A*

Frolov, V. P., & Novikov, I. D. 1998, *Black Hole Physics*, Kluwer Academic Publishers, Fundamental Theories of Physics

Funk, B., et al. 1995, Proc 24th ICRC, Rome, Vol. 2, 104

Gaisser, T. K., & Schaefer, R. K. 1992, *ApJ*, 394, 174

Ghez, A.M., Klein, B. L., Morris, M., Becklin, E. E., 1998, *ApJ* 509, 678

Gibbons, G. W. 1975, *Comm. Math. Phys.*, 44, 245

Giudice, G. F., Kolb, E. W., & Riotto, A. 2001, *Phys.Rev. D*, 64, 023508

Golubkov, D. Yu., Golubkov, Yu. A., & Khlopov, M. Yu., 2000, *Gravitation & Cosmology*, vol 6, supplement, pp 101-106

Gondolo, P. & Silk, J., 1999, *PRL*, 83, 1719

Gradshteyn, I.S., Ryzhik, I.M., 1980, *Table of Integrals, Series, and Products*, Academic Press

Halzen, F., Zas, E., MacGibbon, J. H., & Weeks, T. C. 1991, *Nature*, 353, 31

Han, J. L., Manchester, R. N., Berkhuijsen, E. M., & Beck, R. 1997, *A&A*, 322, 98

Harrison, E. R. 1970, *Phys. Rev. D*, 1, 2726

Hawking, S. W. 1971, *MNRAS*, 152, 75

Hawking, S. W. 1974, *Nature*, 248, 30

Hawking, S. W. 1975, *Comm. Math. Phys.*, 43, 199

Hawking, S. W. 1982, *Phys. Rev. D*, 26, 2681

Hawking, S. W. 1989, *Phys. Lett. B*, 231, 237

Heckler, A. F. 1997, Phys. Rev. D, 55, 480

Kanazawa, T., Kawasaki, M., & Yanagida, T. 2000, Phys. Lett. B, 482, 174

Kim, H. I. 2000, Phys. Rev. D, 62, 063504

Kotok, E., & Naselsky, P. 1998, Phys. Rev. D, 58, 103517

MacGibbon, J. H., & Carr, B. J. 1991, ApJ, 371, 447

MacGibbon, J. H., & Webber, B. R. 1990, Phys. Rev. D, 31, 3052

Maeno, T., *et al.* (BESS Coll.), astro-ph/0010381

Maki, K., Mitsui, T., & Orito, S. 1996, Phys. Rev. Lett., 76, 19

Maurin, D., Donato, F., Taillet, R., & Salati, P. 2001, ApJ, 555, 585 (Paper I)

McDonald, J. 2000, Phys. Rev. Lett., 84, 4798

Mitsui, T., Maki, K., & Orito, S. 1996, Phys. Lett. B, 389, 169

Moore, B., Ghigna, S., Governato, F., Lake, G., Quinn, T., Stadel, J., & Tozzi, P., 1999, ApJ. Lett. 524, L19

Nakamura, T., Sasaki, M., Tanaka, T., & Thorne, K.S. 1997, ApJ, 487, L139

Navarro, J. F., Frenk, C. S. , & White, S. D. M., 1996, ApJ, 462, 563

Niemeyer, J. C., & Jedamzik, K. 1999, Phys. Rev. D, 59, 124013

Orito, S. *et al.* (BESS Coll.) Phys. Rev. Lett. 2000, 84, 1078

Orito, S., Maeno, T., Matsunaga, H., et al., 2001, Adv. Space Res., 26, 1847

Page, D. N., 1976, PhD thesis, Caltech

Page, D. N., 1977, Phys. Rev. D, 16, 2402

Parikh, M. K., & Wilczek, F. 2000, Phys. Rev. Lett., 85, 24

Press, W.H., Teukolsky, S.A., Vetterling, W.T., Flannery, B.P., 1992, Numerical recipes in C, Cambridge University Press

Straulino, S., et al. , 2001, "9th Vienna Conference on Instrumentation" - 19-23 February 2001, Vienna, Austria.

Tjöstrand, T., 1994, Comput. Phys. Commun., 82, 74

Webber, W. R., Lee, M. A., & Gupta, M. 1992, ApJ, 390, 96